

# Restoration of underwater images using depth and transmission map estimation, with attenuation priors

Jarina Raihan A.<sup>\*</sup>, P.G. Emeroylariffion Abas and Liyanage C. De Silva

*Faculty of Integrated Technologies, Universiti Brunei Darussalam,  
Jalan Tungku Link, Gadong BE 1410, Brunei Darussalam*

*(Received March 8, 2021, Revised August 16, 2021, Accepted September 3, 2021)*

**Abstract.** Underwater images are very much different from images taken on land, due to the presence of a higher disturbance ratio caused by the presence of water medium between the camera and the target object. These distortions and noises result in unclear details and reduced quality of the output image. An underwater image restoration method is proposed in this paper, which uses blurriness information, background light neutralization information, and red-light intensity to estimate depth. The transmission map is then estimated using the derived depth map, by considering separate attenuation coefficients for direct and backscattered signals. The estimated transmission map and estimated background light are then used to recover the scene radiance. Qualitative and quantitative analysis have been used to compare the performance of the proposed method against other state-of-the-art restoration methods. It has been shown that the proposed method can yield good quality restored underwater images. The proposed method has also been evaluated using different qualitative metrics, and results have shown that method is highly capable of restoring underwater images with different conditions. The results are significant and show the applicability of the proposed method for underwater image restoration work.

**Keywords:** attenuation coefficients; depth estimation; image restoration; transmission map estimation; underwater images

---

## 1. Introduction

A large part of the earth is covered with water, and underwater life plays an important role in the ecosystem. Therefore, it is very important to explore and discover the underwater world, and one of the ways that this can be done is, by capturing and collecting underwater images and videos. These pictures and videos can be used to explore the underwater world, and can also be used in underwater studies, underwater archaeology, marine ecology, assisting aquatic robots, species recognition, target detection, and underwater geology. As such, there is a requirement for the underwater data collection to be of high accuracy and high quality for proper interpretation of the information.

However, due to the optical properties of water, the quality of the collected underwater images may be relatively poor. The red light from the visible spectrum is quickly absorbed and loses its strength, even in the first part of the ocean which is within 10m depth. It is for this reason; underwater images are commonly dominated by green and blue underwater shades. Deeper into the ocean,

---

<sup>\*</sup>Corresponding author, Research Scholar, E-mail: jari3010@yahoo.in

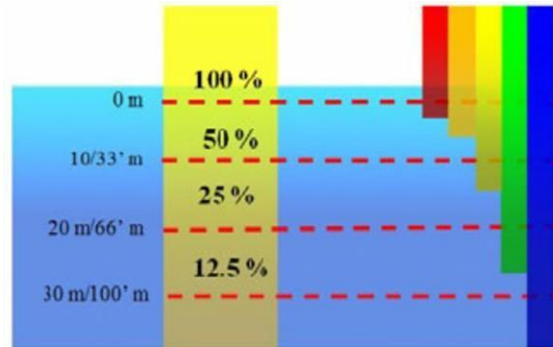


Fig. 1 Light absorption in water and penetrating levels of different colors (Chiang and Chen 2012)

orange, yellow, green, and blue lights from the visible spectrum are also absorbed by the water and cannot penetrate any further. Fig. 1 shows the light absorption property in water and penetrating levels of lights (Chiang and Chen 2012), at various depths. Other than absorption, scattering, diffraction, and polarization may also cause serious problems in the images. Scattering leads to low visibility in clear water, with almost no visibility in turbid water. All these varying properties, which differ at various depths and underwater conditions, make underwater images challenging to recover, and to decrypt their information. Even though artificial lighting may be used to tackle poor visibility, it may cause loss of information in the background, and unnaturally concentrates the illumination on the foreground pixels. Due to these problems, processing of underwater images is the need of the hour, and is required for various studies and scientific researches.

Jarina *et al.* (2019) have provided a review of various underwater image restoration methods that are available in the literature; generally classifying underwater restoration methods into hardware, software, and network-based approaches.

The hardware-based approach employs various hardware to process underwater images for restoration purposes. These include range-gated imaging techniques (Tan *et al.* 2006), polarizers (Schechner and Karpel 2005), imaging using stereo cameras (Roser *et al.* 2014), and remotely operated vehicles (Zhishen *et al.* 2003). Information captured using the selected hardware is then processed using different methods for the restoration of the underwater images. However, these methods have been shown to suffer from errors caused by the calibration of the hardware devices.

The network-based approach involves the use of deep learning algorithms to process underwater images. Convolutional neural networks (Lu *et al.* 2018, Saeed *et al.* 2018) and generative adversarial networks (Fabbri *et al.* 2018, Li *et al.* 2017) are some of the neural networks that have been used for this purpose. However, deep learning methods commonly require a good dataset with a large number of underwater images, together with ground truth images, which are very difficult to acquire, in the case of underwater image processing.

The software-based approach uses the Image Formation Model (IFM) to restore the captured underwater images, by finding background light and transmission maps. Dark Channel Prior (DCP), as proposed by He *et al.* (2011), uses IFM in image restoration, by assuming scene points closer to the camera as dark images and vice versa. But, due to the longer wavelength and faster attenuation property of red light, the method often fails to give proper results, and always ends up choosing the red channel as the darkest of all the channels. Variations of DCP have consequently been proposed

for underwater images; using green and blue channels only (Wen *et al.* 2013, Drews *et al.* 2013, Simon *et al.* 2015), using the inverse of the red channel (Galdran *et al.* 2015), and using the maximum intensity prior (Carlevaris *et al.* 2010). The performances of these methods have been shown to vary depending on different lighting conditions and priors chosen. Instead of estimating the transmission map directly, Peng and Cosman (2017) use a depth estimation strategy that has been proven to show superior results. However, the authors have also shown that depth map, as well as transmission map, need to be efficiently estimated, to obtain satisfactory restoration results.

Other than restoration and enhancement methods, few methods have also analyzed underwater images directly based on edge detection techniques, in order not to capture all the feature information in an image. This is done to distinguish the objects in the water, and to capture the underwater environment information. A bi-dimensional empirical mode decomposition technique has been used by Bo and Liu (2012) to extract multi-pixel edge features and to analyze objects in the image. Instead of a manual choice of threshold parameters, a feature detection algorithm based on ROC theory has been proposed by Bo (2016), to extract the multiscale edges.

To overcome the problems in the above methods, this paper proposes a novel underwater image restoration method by utilizing a single-view image only, and without requiring large prior image datasets. It has been shown that the proposed method can properly restore underwater images, with good accuracy when compared to the ground truth as well as to other states of the art methods. The proposed software-based image restoration method utilizes blurriness information, and background light neutralization to find a depth map, which is then employed to find the transmission map. The transmission map then undergoes a refinement process and finally, is restored efficiently.

## 2. Literature review

The image restoration process employs the Image Formation Model (IFM) given in Eq. (1), to obtain the original scene from a captured underwater scene. This process involves estimating the different parameters of the underwater IFM in Eq. (1).

$$I^c(x) = J^c(x).t^c(x) + (1 - t^c(x)).B^c, \quad c \in \{R, G, B\} \quad (1)$$

In the above equation,  $J^c(x).t^c(x)$  describes radiance  $J^c(x)$  of the object as it travels in the underwater medium, whilst  $(1 - t^c(x)).B^c$  represents the scattering of background light  $B^c$  as it travels towards the camera. Transmission map  $t^c(x)$  describes the part of the object radiance that reaches the camera, after considering for absorption and scattering. Recovering the original object radiance  $J^c(x)$  from the acquired image  $I^c(x)$  at the camera requires knowledge of the background light  $B^c$  as well as the transmission map  $t^c(x)$ . This information is commonly estimated.

Dark Channel Prior (DCP), originally introduced by He *et al.* (2011), uses Eq. (2) to estimate the intensity of the dark channel, from  $I^c(x)$ . This is given by

$$I_{dark}^c(x) = \min_{y \in \Omega(x)} \left\{ \min_c I^c(y) \right\}, \quad c \in \{R, G, B\} \quad (2)$$

where  $\Omega(x)$  is the square patch centred at  $x$ .

Background light  $B^c$  and transmission map  $t^c(x)$  are subsequently determined using Eqs. (3) and (4), to give the estimated background light  $\widetilde{B}^c$  and the estimated transmission map  $\widetilde{t}^c$ ,

respectively (Chiang and Chen 2012, Liu *et al.* 2010, Yang *et al.* 2011). These estimates can then be used to estimate radiance  $\tilde{J}^c(x)$  of the object using Eq. (5).

$$\tilde{B}^c = I^c \left( \operatorname{argmax}_{x \in P_{0.1\%}} \sum_c I^c(x) \right), \quad c \in \{R, G, B\} \quad (3)$$

$$\tilde{t}^c(x) = 1 - \min_{y \in \Omega(x)} \left\{ \min_c \frac{I^c(y)}{B^c} \right\}, \quad c \in \{R, G, B\} \quad (4)$$

$$\tilde{J}^c(x) = \frac{I^c(x) - \tilde{B}^c}{\max(\tilde{t}^c(x), t_0)} + \tilde{B}^c, \quad c \in \{R, G, B\} \quad (5)$$

where the lower bound  $t_0$  for  $\tilde{t}^c(x)$ , is set to 0.1.

Transmission map estimations for DCP based methods (Liu *et al.* 2010, Yang *et al.* 2011, Chiang and Chen 2012, Wen *et al.* 2013, Drews *et al.* 2013, Galdran *et al.* 2015) commonly follow Eq. (4), with few variations for underwater images. But the DCP methods work only in limited conditions and since underwater images have varying conditions, these methods often fail to accurately estimate the transmission map for challenging conditions.

An alternative to estimating transmission map using Eq. (4) is by considering the object's distance from the camera  $\tilde{d}(x)$  or its depth, and the water attenuation coefficient  $\beta^c$  in colour channel  $c \in \{R, G, B\}$

$$\tilde{t}^c(x) = e^{-\beta^c \tilde{d}(x)}, \quad c \in \{R, G, B\} \quad (6)$$

Methods proposed in references (Peng and Cosman 2017, Chang *et al.* 2019) estimate the transmission map using Eq. (6); which is more efficient as compared to estimating transmission map directly using Eq. (4). Fig. 2 shows a qualitative comparison of restoration results obtained using methods with and without depth estimation to determine transmission maps (Peng and Cosman 2017).

Carlevaris *et al.* (2010) have proposed a method for estimating depth and consequently, to restore underwater images. The authors have estimated the depth map of an acquired image using Eq. (6), by assuming a certain spectral attenuation coefficient  $\beta^c$  value, which largely depends on water type. Attenuation prior difference between the three-color channels, by considering the channel with the maximum intensity, has been utilized by Carlevaris *et al.* (2010). Chiang and Chen (2012) have used DCP for underwater image restoration; using fixed attenuation coefficient measured for open ocean water. But, since DCP relies on the assumption which always ends up choosing the red channel, the restoration results do not give satisfactory outcomes.

Peng *et al.* (2015) have proposed a method using blurriness information for depth map estimation. This depth map estimation is then used to find a transmission map of the underwater image using Eq. (6), by selecting attenuation coefficients  $\beta^c$ , as defined by Zhao *et al.* (2015).

To capture an underwater image, light from the object of interest should reach the camera. Light travelling directly from the object without any interference is referred to as a direct signal, whilst light that reflects back to the camera's lens of focus, due to its interactions with particles in the water medium is referred to as a backscattered signal. Backscattered signals, undergo scattering in an underwater environment due to interactions between the photons, molecules and particles of the medium. Major sources of distortion for backscattering signals are viruses, bacteria, suspended particulate matter, bubbles, phytoplankton, zooplankton, and soluble substances. Due to the different



Fig. 2 Examples of restoration results of Peng and Cosman (2017) with and without depth estimation

sources of distortion experienced by direct and backscattered signals, it is very important to consider both signals separately; by accounting for the effect of scattering using separate attenuation coefficients for the two signals.

However, the general transmission map estimation in the literature (Peng and Cosman 2017, Chang *et al.* 2019), commonly, employs a single spectral coefficient  $\beta^c$  for transmission map estimation using Eq. (6). Somehow, they neglect the effects of different distortions from the two distinct signals: direct and backscattered signals, resulting in less efficient scene restoration (Akkaynak and Trebitz 2018). Separate estimations of transmission maps utilizing different attenuation coefficient values for the two signals, have to be made, for an efficient result.

Furthermore, it is common to assume an identical attenuation coefficient i.e.,  $\beta^R = \beta^G = \beta^B$  for the different color channels: red, green and blue. For hazy terrestrial images, transmission estimation is based on three assumptions: overcast lighting, spatially invariant attenuation coefficients, and wavelength-independent attenuation (Narasimhan *et al.* 2002). However, natural underwater illumination undergoes a color-dependent attenuation; violating the original wavelength-independent attenuation assumption of terrestrial images. The method proposed in this paper differentiates the effect of direct and backscattered lights, as well as the effect on the different color channels.

### 3. Proposed image restoration method

The proposed method involves five stages: blurriness estimation, background light neutralization, depth estimation, transmission estimation along with transmission map refinement, and finally, scene radiance recovery, as shown in Fig. 3. Red-light intensity  $I^r(x)$ , blurriness estimated image  $p_{\text{blr}}$  and background light neutralized image  $\tilde{B}^c$ , are calculated from the input image  $I^c(x)$ . These are then used to estimate the depth  $\tilde{d}(x)$  of the underwater image. The depth map  $\tilde{d}(x)$  along with selected spectral attenuation coefficients is then used to determine the transmission map  $\tilde{t}^c(x)$ . The input image  $I^c(x)$ , estimated background light  $\tilde{B}^c$  and transmission map  $\tilde{t}^c(x)$  are used to find the final scene radiance recovered image  $\tilde{J}^c(x)$ .

The novelty of the approach lies in the simplified way of estimating background light using the 4 quadrants subdivision process, as well as the estimation of transmission map, using an aggregate

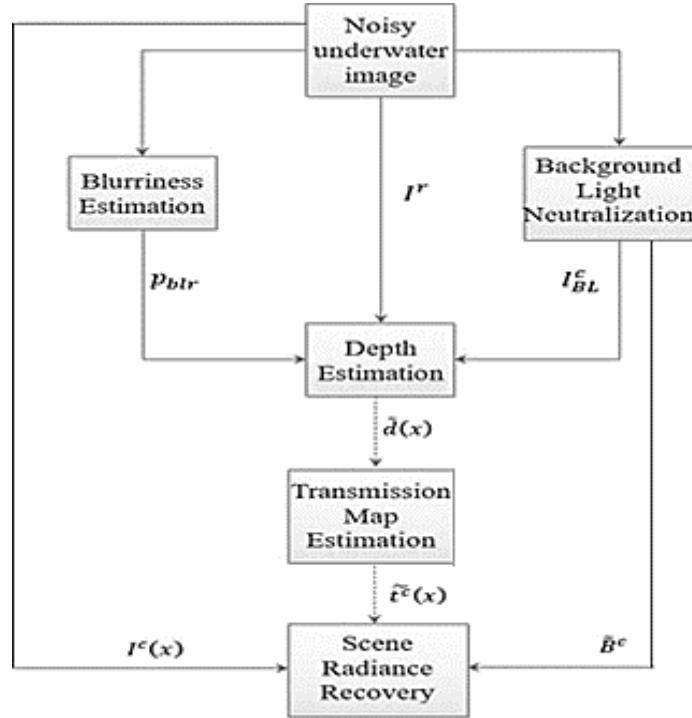


Fig. 3 Block diagram of the proposed restoration method

of transmission maps found for direct signal and backscattered signal using specified attenuation coefficients. This is unlike other methods which commonly use Eq. (2); by assuming a general water attenuation coefficient  $\beta^c$  for the transmission map estimation.

### 3.1 Blurriness estimation background light estimation, background light neutralization and depth estimation

The blurriness map estimation  $p_{blr}$  is the first process in the restoration process, by estimating the refined blurriness map, through the initial map and rough map of the image (Peng and Cosman 2017). The background light estimation is the selection or estimation of the pixel, which is responsible for the source of light to the entire image. To determine the background light, the input image  $I^c(x)$  is segmented into 4 quadrants, with mean value of pixels calculated, which represents the least number of quadrant sub-divisions that can be made, and hence, is simpler and more efficient, with reduced computational processing time as, compared to the method in reference (Peng and Cosman 2017). Eq. (7) is used to estimate background light  $\tilde{B}^c$

$$\tilde{B}^c = \max(I_{q_{BL}}^c(x)) \quad (7)$$

$$\text{where, } I_{q_{BL}}^c = q_{mid} \quad q_{mid} \in \{q_{i=\{1,2,3,4\}} - q_{max} - q_{min}\} \quad (8)$$

The selected pixel, which constitutes the estimated background light  $\tilde{B}^c$ , may not be the brightest of all pixels in the entire input image, as the two quadrants have been excluded from the selection process. The estimated background light  $\tilde{B}^c$  shall be used for the scene radiance recovery using Eq. (6).

For the background light estimation process, the original input underwater image  $I^c(x)$  is segmented into 4-quadrants, with the mean of pixel intensities at each quadrant calculated using

$$I_{q_i}^c = avg_{x \in q_i} (\sum_c I^c(x)) \quad (9)$$

Background light neutralized image  $I_{BL}^c(x)$  needs to be estimated to find the depth map of the underwater image. Initially, average light intensity  $I_{q_{avg}}^c$  in the two quadrants, excluding the two extremes, is determined, and taken as the average of the underwater image

$$I_{q_{avg}}^c = avg_{q_i \in q_{mid}} (I_{q_i}^c) \quad (10)$$

where  $q_i$  is the four quadrants  $i = 1, 2, 3, 4$ , with  $I_{q_i}^c$  representing the average light intensity in the respective quadrant  $q_i$ . The brightest  $q_{max}$  and darkest  $q_{min}$  quadrants are neglected, as two extremes of the spectrum.

This average light intensity  $I_{q_{avg}}^c$  is then used to modify all the pixels of the input image  $I^c(x)$  to retrieve the contrast neutralized image  $I_{cn}^c(x)$ , as follows

$$I_{cn}^c(x) = I^c(x) + I_{q_{avg}}^c \quad (11)$$

To denoise the image, discrete wavelet transform (DWT) is applied on the currently formed contrast neutralized image  $I_{cn}^c(x)$ , and the Gray version of the input image  $I^c(x)$ . Inverse discrete wavelet transform (IWDWT) is finally applied to retrieve the background light neutralized image, with the approximation and the detailed coefficients modified based on the average of the approximation coefficients, and the max rule applied on the detailed coefficients.

The blurriness map, the background light neutralized image, and the intensity of the red channel can be used for the depth estimation process (Jarina *et al.* 2020). The maximum intensity of the red channel, known as red channel map  $r(x)$  of the image, is represented by

$$r(x) = \max_{y \in \varphi(x)} I^r(y) \quad (12)$$

where,  $I^r$  is the intensity of the red channel and  $\varphi(x)$  is a square local patch centered at  $x$ .

The factors used for estimating depth are passed through a stretching function that is given by Eq. (13) (Jarina *et al.* 2020).

$$d_{f(x)}(x) = 1 - F_s(f(x)), \quad f(x) \in \{r(x), p_{blr}(x), I_{BL}^c(x)\} \quad (13)$$

where,  $f(x) \in \{r(x), p_{blr}(x), I_{BL}^c(x)\}$  can either be the red channel map  $r(x)$ , blurriness map  $p_{blr}(x)$  or background neutralised image  $I_{BL}^c(x)$ , to give  $d_r(x)$ ,  $d_{p_{blr}}(x)$  and  $d_{I_{BL}^c}(x)$ , respectively.

$$F_s(\mathbf{v}) = \frac{\mathbf{v} - \min(\mathbf{v})}{\max(\mathbf{v}) - \min(\mathbf{v})} \quad (14)$$

where,  $f(x) \in \{r(x), p_{blr}(x), I_{BL}^c(x)\}$  can either be the red channel map  $r(x)$ , blurriness map  $p_{blr}(x)$  or background neutralised image  $I_{BL}^c(x)$ , to give  $d_r(x)$ ,  $d_{p_{blr}}(x)$  and  $d_{I_{BL}^c}(x)$ ,

respectively.  $F_s(\mathbf{v})$  is a stretching function, which accepts vector  $\mathbf{v}$  as its input. The final depth estimation can be found by Eq. (15)

$$\tilde{d}(x) = \theta_b \left[ \theta_a d_{I_{BL}^c}(x) + (1 - \theta_a) d_r(x) \right] + (1 - \theta_b) d_{p_{blr}} \quad (15)$$

where,  $f(x) \in \{r(x), p_{blr}(x), I_{BL}^c(x)\}$  can either be the red channel map  $r(x)$ , blurriness map  $p_{blr}(x)$  or background neutralised image  $I_{BL}^c(x)$ , to give  $d_r(x)$ ,  $d_{p_{blr}}(x)$  and  $d_{I_{BL}^c}(x)$ , respectively.  $F_s(\mathbf{v})$  is a stretching function, which accepts vector  $\mathbf{v}$  as its input where,  $f(x) \in \{r(x), p_{blr}(x), I_{BL}^c(x)\}$  can either be the red channel map  $r(x)$ , blurriness map  $p_{blr}(x)$  or background neutralised image  $I_{BL}^c(x)$ , to give  $d_r(x)$ ,  $d_{p_{blr}}(x)$  and  $d_{I_{BL}^c}(x)$ , respectively.  $F_s(\mathbf{v})$  is a stretching function, which accepts vector  $\mathbf{v}$  as its input where,  $\theta_a$  and  $\theta_b$  are  $\theta_a = S(\text{avg}(I_{BL}^c), 0.5)$  and  $\theta_b = S(\text{avg}(I^r), 0.1)$ , respectively. The values 0.5 and 0.1 for  $\theta_a$  and  $\theta_b$  have been obtained from Peng and Cosman (2017), and the effectiveness of the values in the restoration process has been verified. The  $\text{avg}(\cdot)$  function gives the average of the input, whilst the sigma function  $S(a, v)$  is given as

$$S(a, v) = \left[ 1 + e^{-s(a-v)} \right]^{-1} \quad (16)$$

### 3.2 Transmission map estimation and scene recovery or restoration

Peng and Cosman (2017) have given importance only to the direct signals, by estimating transmission map by considering the spectral attenuation coefficient of direct signal  $\beta_D^c$  only, whilst neglecting the backscattered signal. In the proposed method, transmission map estimation separates the effects of direct and backscattered signals. Transmission map estimations are accomplished by using two different spectral attenuation coefficients  $\beta_D^c$  and  $\beta_B^c$ , where  $\beta_D^c$  is the spectral attenuation coefficient of the direct signal and  $\beta_B^c$  is the spectral attenuation coefficient of the backscattered signal given as

$$\tilde{t}^c(x) = t_D^c(x) + t_B^c(x), \quad c \in \{R, G, B\} \quad (17)$$

Generally, attenuation coefficients vary with depth  $d(x)$ , as stated in Akkaynak and Tretbitz (2018), where it has more role to play with the restoration of images.

#### 3.2.1 Estimation of $\beta_D^c$

The transmission map of the direct signal is estimated using spectral attenuation coefficients calculated for red, green and blue channels, together with the calculated depth map  $\tilde{d}(x)$ . The transmission map for the red channel can be calculated using

$$t_D^r(x) = e^{-\beta_D^r \tilde{d}(x)} \quad (18)$$

Restoration results are not sensitive to the spectral attenuation coefficient  $\beta_D^r$  of the red channel (Peng and Cosman 2017), with values between [0.125, 0.20] commonly used for oceanic water type I (Solonenko *et al.* 2015). Consequently, in this paper, the spectral coefficient value  $\beta_D^r$  of the red channel is set with a value of 0.142. To find the transmission map for the green and blue channels due to direct signal, transmission and attenuation coefficient for the red channel may be utilized (Zhao *et al.* 2015), as given by,

$$t_D^k(x) = t_D^r(x)^{\frac{\beta_D^k}{\beta_D^r}}, \quad k \in \{g, b\} \quad (19)$$

The linear relationship between the attenuation coefficients of the green/blue channels and the red channel, is given by Eq. (20), where constants  $m$  and  $i$  are the absorption and scattering coefficient constants, with values  $m = -0.00113$ , and  $i = 1.62517$  (Gould *et al.* 1999). These values have been determined, by developing the linear relationship using a laboratory apparatus using case 1 and case 2 of Jerlov water types. Wavelength for the red, green and blue light is taken to be 620 nm, 540 nm, and 450 nm, respectively (Peng and Cosman 2017).

$$\frac{\beta_D^k}{\beta_D^r} = \frac{\tilde{B}^r (m\lambda^k + i)}{\tilde{B}^k (m\lambda^r + i)} \quad k \in \{g, b\} \quad (20)$$

here,  $\tilde{B}^k$  is the background light estimated using Eq. (7), for the respective channel  $k \in \{g, b\}$ .

### 3.2.2 Estimation of $\beta_B^c$

The backscattering coefficient is dependent on organic and inorganic particulate matters. Organic particulate matter includes viruses, bacteria, phytoplankton and zooplankton species, whilst inorganic particulate matter are suspended sediments, debris, clay and minerals. Air bubbles are also high sources of backscattering in water. Spectral attenuation backscattering has important applications in the interpretation of remote sensing, oceanography, underwater imaging (Shanmugam *et al.* 2011). Total backscattering coefficient  $\beta_B^c$  is a summation of pure water backscattering coefficient  $\beta_{BW}^c$  and particulate matter backscattering coefficient  $\beta_{BP}^c$

$$\beta_B^c(\lambda) = \beta_{BW}^c(\lambda) + \beta_{BP}^c(\lambda) \quad (21)$$

Comprehensive researches have been made on the estimation of spectral attenuation backscattering coefficients, with Mie theory used to predict spectral behaviour. Whitmire *et al.* (2007) have used Slow Descent Rate Optical Profiler (Slow DROP), to experimentally calculate the backscattering coefficient of particulate matters in five research cruises at five different wavelengths covering the visible spectrum, for three years. Smith *et al.* (1981) have used UV submersible Spectro-radiometer to calculate the total backscattering coefficient of pure water at thirteen different wavelengths. Pure water backscattering coefficient  $\beta_{BW}^c$ , particulate matter backscattering coefficient  $\beta_{BP}^c$ , and total backscattering coefficient  $\beta_B^c$ , for the wavelength of the red, green and blue light, are shown in Table 1. Pure water backscattering coefficient  $\beta_{BW}^c$  and particulate matter backscattering coefficient  $\beta_{BP}^c$  are taken from reference (Whitmire *et al.* 2007). Total backscattering attenuation coefficients for each desired wavelength are then calculated using Eq. (21).

Transmission map due to backscattered signal, may be derived from Eqs. (6) and (21) as follow

$$t_B^r(x) = e^{-\beta_B^c \cdot \tilde{d}(x)} \quad c \in \{r, g, b\} \quad (22)$$

Spectral attenuation coefficients of the direct  $\beta_D^c$  and backscattered  $\beta_B^c$  signals, may be used to estimate the raw transmission map, using Eq. (22). The estimated transmission is then further refined by using the guided filter (He *et al.* 2013), instead of soft matting (He *et al.* 2011), because of its better refinement properties.

Table 1 Determining the total backscattering attenuation coefficient  $\beta_B^c(\lambda)$ 

Wavelength	$\beta_{BW}^c(\lambda)$ (Smith <i>et al.</i> 1981)	$\beta_{BP}^c(\lambda)$ (Whitmire <i>et al.</i> 2007)	$\beta_B^c(\lambda)$
450 nm	0.0022	0.0175	0.0197
540 nm	0.0010	0.0126	0.0136
620 nm	0.0006	0.0133	0.0139

Scene radiance recovery involves the use of the estimated background light and transmission map to form the final scene radiance. The refined transmission map is used in Eq. (5) to acquire the final restored image.

## 4. Results and discussions

### 4.1 Performance metrics and dataset used

The proposed method has been tested with four quality metrics; to ascertain its performance.

1 Visibility recovery  $e$  and restoration quality  $r$  coefficients

$$e = \frac{n_r - n_o}{n_o} \quad (23)$$

where,  $n_r$  indicates the number of edges calculated using Canny operator in restored image and  $n_o$  detects the edges calculated in the original image.

$$r = \frac{1}{n_r} \sum_i \log(I^c(i)) \quad (24)$$

For each pixel  $i$  belonging to a visible edge, restoration quality  $r$  computes the average ratio of the gradient in the restored image  $\tilde{J}_C(x)$  and in the original image  $I^c(x)$ .

### 2. Mean Squared Error (MSE)

Mean Squared Error (MSE) is a measure of collective squared error between the original image and the restored image. This value should be low for a good restored image.

$$MSE = \frac{1}{M} * \sum_{x=1}^M (I^c(x) - \tilde{J}_C(x))^2 \quad (25)$$

where,  $M$  is the dimension of the image,  $I^c(x)$  is the original image and  $\tilde{J}_C(x)$  is the restored image.

### 3. Underwater Colour Image Quality Evaluation (UCIQE) (Yang and Sowmya 2015)

Underwater Colour Image Quality Evaluation (UCIQE) may be used to measure how well the blurriness and overall contrast of the restored image have been reduced; with a high UCIQE value

implying quality enhancement. It is represented by

$$UCIQE = C_1 * \sigma_c + C_2 * con_l + C_3 * \mu_s \quad (26)$$

where,  $C_1 = 0.4680$ ,  $C_2 = 0.2745$ , and  $C_3 = 0.2576$ .  $\sigma_c$ ,  $con_l$  and  $\mu_s$  are the standard deviation of chroma, the contrast of luminance and the average of saturation of the restored image, respectively (Yang and Sowmya 2015).

#### 4. Underwater Image Quality Measure (UIQM) (Panetta *et al.* 2016).

Underwater Image Quality Measure (UIQM) is a combined measure of colour, sharpness and contrast of the restored underwater image. Increase UIQM value implies increase in quality.

$$UIQM = C_1 * UICM + C_2 * UISM + C_3 * UIConM \quad (27)$$

where,  $C_1 = 0.0282$ ,  $C_2 = 0.2953$ ,  $C_3 = 3.5753$ , and Underwater Image Colourfulness Measure (UICM), Underwater Image Sharpness Measure (UISM), Underwater Image Contrast Measure (UIConM), are the colourfulness, saturation and contrast measures of the image calculated as in reference (Panetta *et al.* 2016). Both UCIQE and UIQM are performance metrics dedicated to underwater images.

Different datasets have been used in the paper, for performance comparison of the proposed method against other methods. This includes an image dataset from Peng and Cosman (2017), Li *et al.* (2019), and Duarte *et al.* (2016). Duarte *et al.* (2016) have provided 3D TURBID dataset; obtained from experimental simulations of underwater scenarios with a 1000 liters tank and fluorescent lamps, for evaluating underwater images. The 3D TURBID dataset uses information on the characteristics and structures of real seabed images, which were obtained from the Bahamas. High-quality images of the seabed were placed at the bottom of the water tank. Simulations were performed by gradually adding milk into the water tank to produce different levels of turbidity, and taking images of the seabed; with the use of two LED lamps to ensure uniform light. Degradation in visual clarity as turbidity is increased, is quantified using Structural Degradation Index (SDI) (Garcia and Gracias 2011); which is defined from Structural Similarity Index (SSIM) (Zhou *et al.* 2004). As the dataset contains reference images, a quantitative evaluation of final restored images using MSE can be made.

#### 4.2 Qualitative analysis and quantitative evaluation

Qualitative analysis involves a visual evaluation of the proposed method against various restoration methods used in the literature. Fig. 4-8 show the restored underwater images with various underwater conditions, using different methods. Different light absorption and penetration level, which affect the color of the underwater images, at varying underwater depth represent one of the main challenges in underwater image restoration work. As such, 5 underwater images with different underwater color tones and lighting conditions, have been selected for the evaluation of the proposed restoration method. All underwater images used has a resolution of 72 dots per inch (dpi). Fig. 4-8 depict underwater images with natural lighting, with bluish shade, with greenish shade, with artificial lighting and backscattering, respectively.

Fig. 4 shows the performance of the proposed method against other methods, in an open scene underwater image with natural lighting. Carlevaris *et al.* (2010) and Chiang and Chen (2012) are unable to remove the greenish color dominance of the original input underwater image. Serikawa *et al.* (2013) produce a similar result with over exposure and increased contrast. On the other hand,

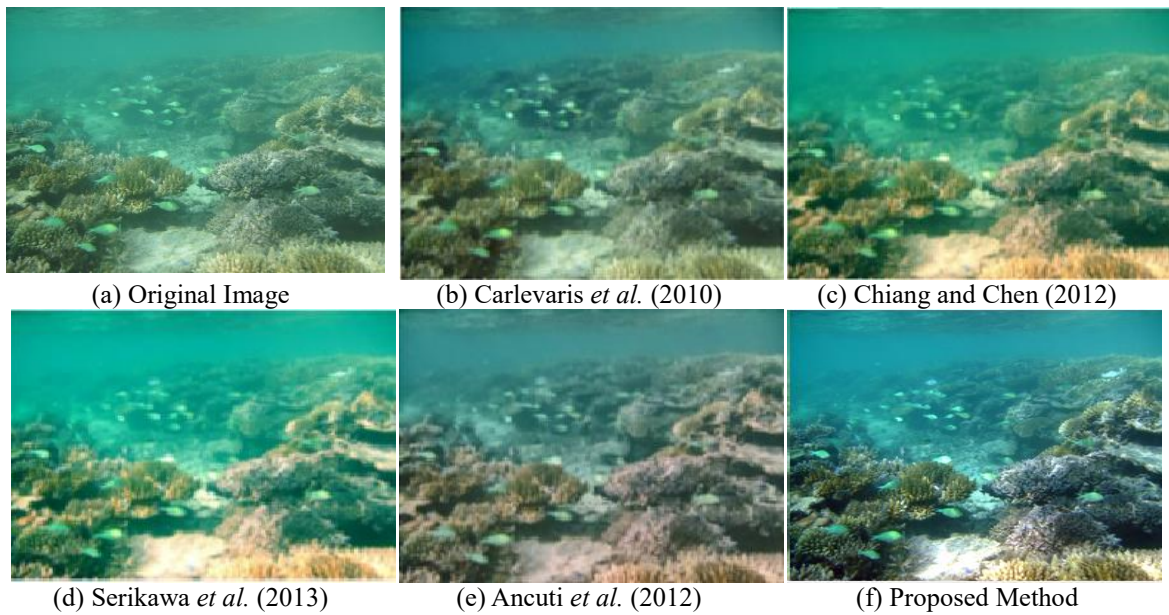


Fig. 4 Results on open scene image

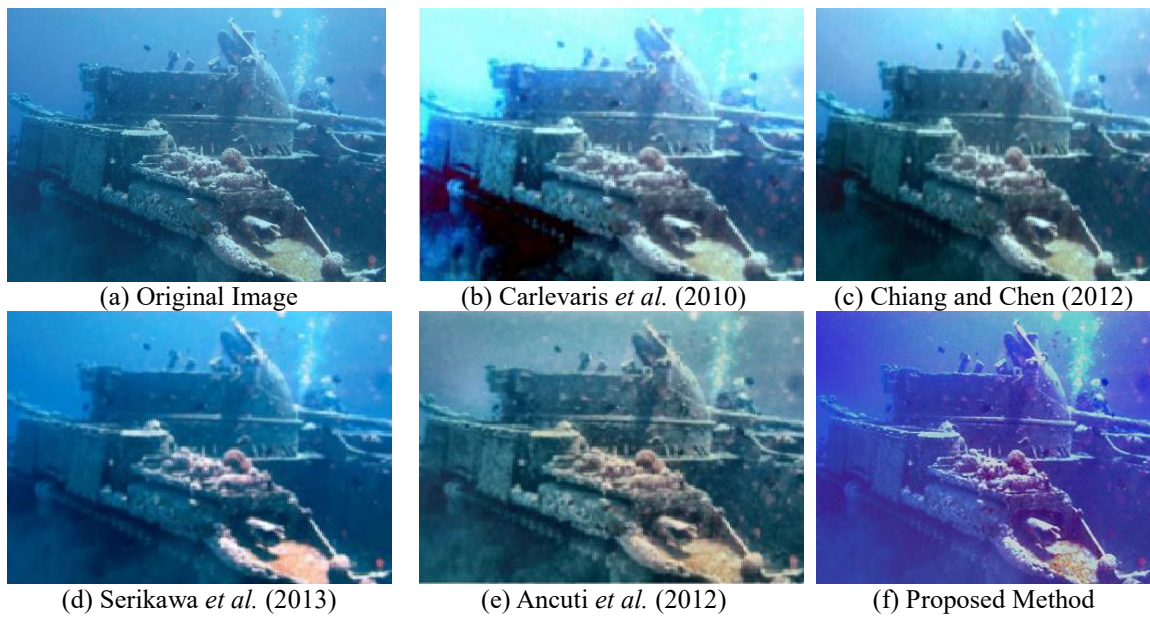


Fig. 5 Results on ship image

Ancuti *et al.* (2012) produce a restored image with a natural look. However, the proposed method shows the best result by removing the color dominance, and exactly depicting places of natural lighting, which are not obtained from restored images using other methods.

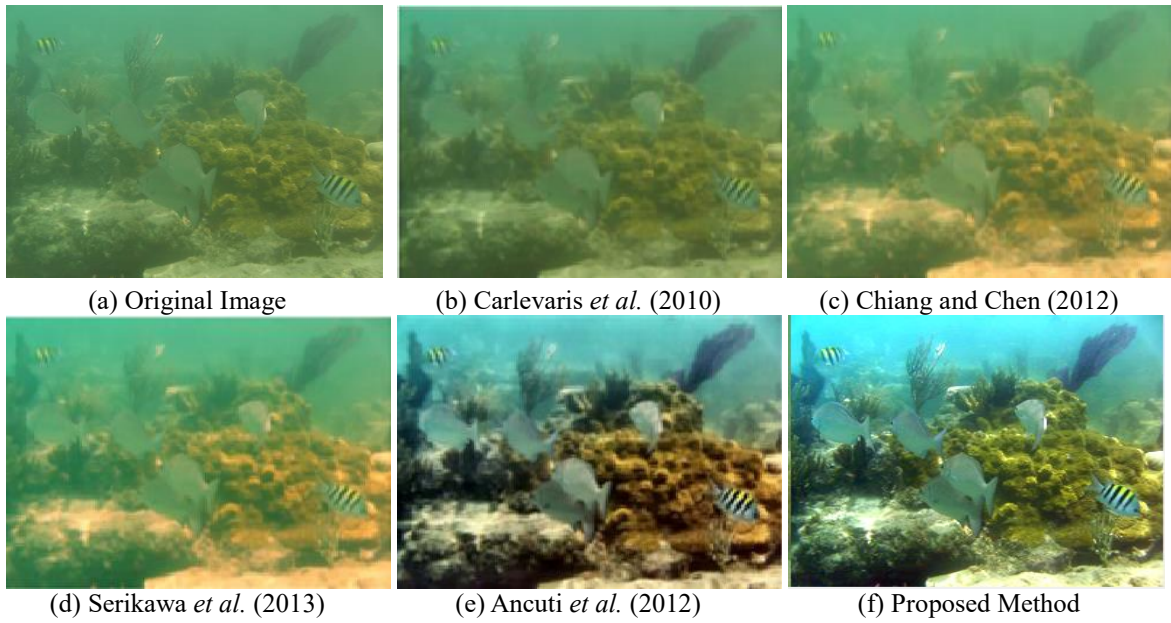


Fig. 6 Results on fishes scene image

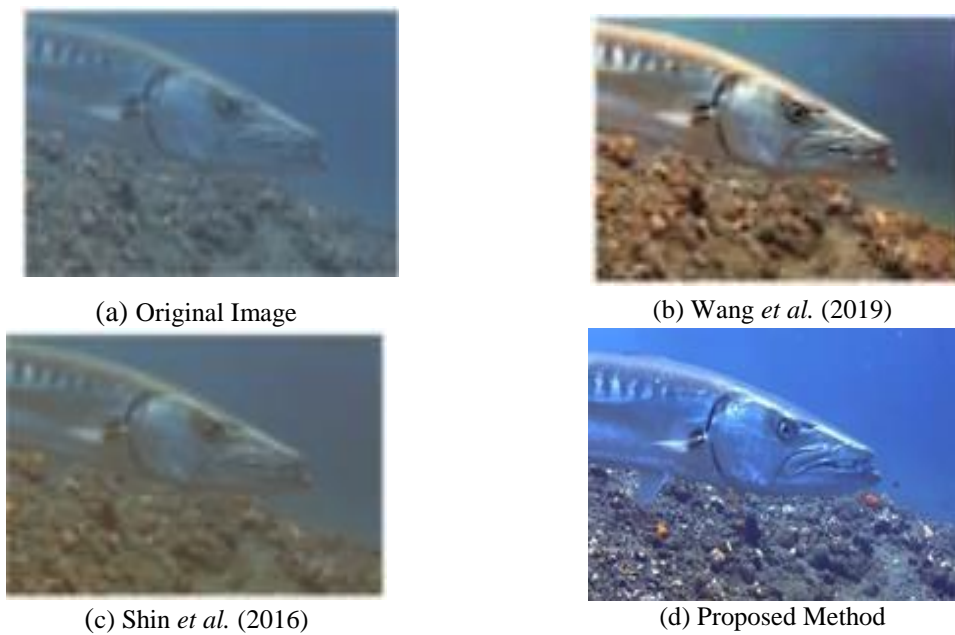


Fig. 7 comparison with network-based methods

Bluish shade is a common imaging phenomenon in underwater images. Fig. 5 depicts a bluish image of a shipwreck under the sea, and its restored results. Carlevaris *et al.* (2010) produce an over exposed image with high contrast, whilst Chiang and Chen (2012) fail to restore the image,



Fig. 8 comparison on challenging underwater image from Li *et al.* (2019) dataset

producing a low saturated result. On the other hand, the proposed method preserves the original features of the image, with its foreground and background pixels correctly classified and restored accordingly.

Fig. 6 shows the underwater greenish image of fishes in a reef. Carlevaris *et al.* (2010) is unable to produce a better restoration result; with the outcome looking identical to the original unrestored underwater image. Serikawa *et al.* (2013) produce a restored underwater image, which emphasizes the brightness of the overall image, whilst leaving the greenish nature still un-cleared. The proposed method deals gracefully with the underwater image, by producing a natural result and also, improving the overall pixel quality.

Fig. 7 compares the performance of the proposed method against network-based methods. It can be seen that the proposed method performs well by preserving the exact color of the image, as well as being able to restore features of the object. Wang *et al.* (2019) restore the underwater image well but are unable to preserve the edges. Shin *et al.* (2016) fail to preserve the color and restores poorly; without any noticeable improvement. This is because network-based methods rely on a good and large training dataset, without which the methods lose their accuracy.

Fig. 8 shows the comparison of the proposed method and its performance on a challenging image with a backscattering effect; where the turtle object in the original underwater image is hidden by the extreme greenish color layer on the image, with minimal information on the turtle object. This image is extracted from Li *et al.* (2019). Drews *et al.* (2013) and Peng and Cosman (2017) fail to restore the original color of the turtle object. Ancuti *et al.* (2012) manage to clear the greenish nature of the image, however, the restored image looks over exposed with high contrast and saturation. The proposed method shows a very good result concentrating on both foreground and background pixels, exposing the original color of the turtle as brown and black, as well as clearly restoring the background sand. As a result of the improved transmission estimation, the image affected by back

Table 2 Visibility recovery coefficient  $e$  of different restoration methods

	Open scene with Natural Lighting (Fig. 4)	Bluish image of a shipwreck (Fig. 5)	Greenish image of fishes in a reef (Fig. 6)
Ancuti <i>et al.</i> (2012)	0.0637	1.4890	7.5038
Carlevaris <i>et al.</i> (2010)	-0.2039	1.3534	0.5354
Chiang and Chen (2012)	0.1705	0.3123	0.1842
Serikawa <i>et al.</i> (2013)	0.1490	0.0381	0.9163
<b>Proposed Method</b>	<b>4.5415</b>	<b>1.9987</b>	<b>18.134</b>

Table 3 Restoration quality coefficient  $r$  of different restoration methods

	Open scene with Natural Lighting (Fig. 4)	Bluish image of a shipwreck (Fig. 5)	Greenish image of fishes in a reef (Fig. 6)
Ancuti <i>et al.</i> (2012)	1.7827	1.4890	0.9813
Carlevaris <i>et al.</i> (2010)	1.3625	2.6018	5.3905
Chiang and Chen (2012)	1.7812	1.7677	1.4304
Serikawa <i>et al.</i> (2013)	2.1414	1.7677	1.4304
<b>Proposed Method</b>	<b>0.4990</b>	<b>0.1740</b>	<b>0.7645</b>

scattering is effectively restored. Over exposure of the image properties, such as brightness and contrast, have also been successfully controlled.

Tables 2 and 3 show visibility recovery coefficients  $e$  and restoration quality coefficients  $r$ , respectively, of the different restoration methods, on underwater images in Figs. 4-6. Figs. 4-6 depict an open scene of an underwater image with natural lighting, a bluish image of a shipwreck under the sea, and a greenish image of fishes in a reef, respectively. Visibility recovery coefficient  $e$  measures whether the method can retrieve the edges that have been lost due to scattering, whilst restoration quality coefficient  $r$  reflects the quality of the restoration. Higher  $e$  value and lower  $r$  value indicate that the restoration method is highly capable of restoring the underwater image.

From the Table 2, Ancuti *et al.* (2012) performs well in retrieving edges of images in Figs. 5 and 6. Visibility recovery coefficients  $e$  of 1.4890 and 7.5308, are obtained for images in Figs. 5 and 6, respectively, using the restoration method by Ancuti *et al.* (2012). This shows that this method can retrieve the edges well in these underwater images. But in Fig. 4, its performance is poor since the image is highly affected by backscattering effect. Other methods by Carlevaris *et al.* (2010), Chiang and Chen (2012), and Serikawa *et al.* (2013), give lower visibility recovery coefficient  $e$ , and are able to recover only a smaller number of edges, as can be confirmed from visual evaluations of Figs. 4-6. The proposed restoration method performs the best on all the three images, capable of recovering the edges, as well as able to correctly estimate the background and foreground pixels. Visibility recovery coefficients  $e$  of 4.5415, 1.9987, and 18.134, for underwater images in Figs. 4-6, respectively, using the proposed method, represent the highest  $e$  values among the restoration methods considered, for all three underwater images.

Table 3 shows the restoration quality coefficient  $r$  values, which measure the directional change in color of a restored image to that of the original image, of different restoration methods for images in

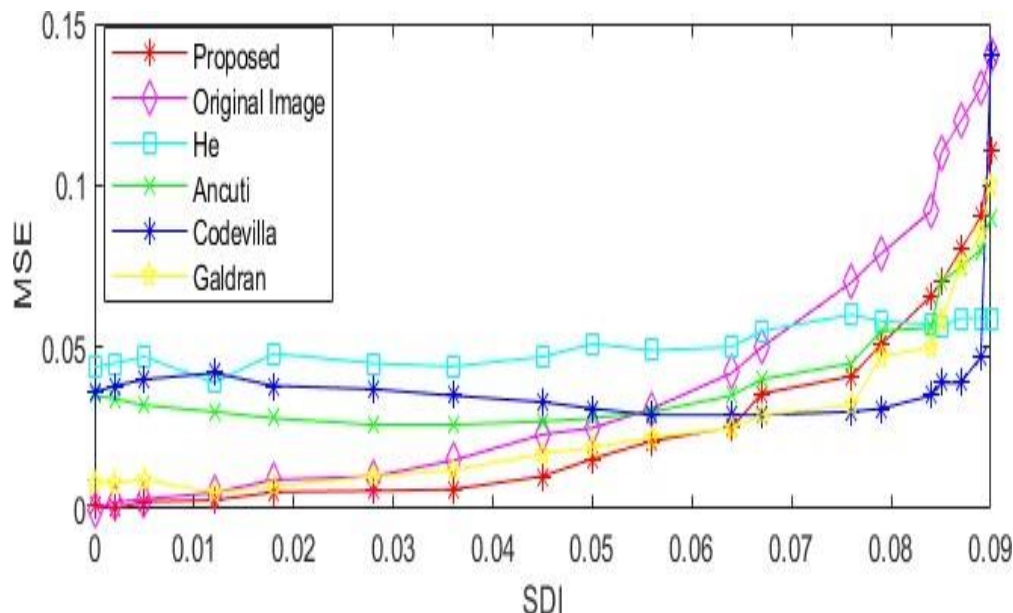


Fig. 9 comparison of various methods on 3D TURBID dataset (Duarte *et al.* 2016)

Figs. 4-6. Since restoration quality coefficient  $r$  is dependent on the visible edges, Ancuti *et al.* (2012) perform well and recover more spurious edges next to the proposed method in Fig. 6. However, its restoration performances are poor in Figs. 4 and 5; albeit it gives better restoration performance than other restoration methods for Fig. 4. Carlevaris *et al.* (2010), Chiang and Chen (2012) and Serikawa *et al.* (2013) have higher restoration quality coefficient values, since they estimate less visible edges i.e., low visibility recovery coefficients  $e$ . The proposed method outperforms other methods, by estimating the visible edges of the underwater images very well, and consequently, giving the lowest restoration quality coefficient  $r$  values for all the 3 images. Restoration quality coefficients  $r$  are 0.4990, 0.1740 and 0.764, for underwater images in Figs. 4, 5 and 6, respectively, using the proposed restoration method.

Fig. 9 compares the performance of the proposed restoration method against other methods, on the 3D TURBID dataset (Duarte *et al.* 2016). The dataset contains 19 simulated underwater images ( $I_i, i=0, 1, \dots, 18$ ); with  $I_0$  having the lowest turbidity and  $I_{18}$  having the highest turbidity. Structural Degradation Index (SDI) (Garcia and Gracias 2011); representing the differences between the turbid image and original ground truth image, has been calculated for each of the images. Different restoration methods were then used to restore the turbid images, with MSE values calculated using the original ground truth images and plotted in Fig. 9. It is noted that for effective restoration, the method must be able to reduce MSE values to that below of the original turbid images line (represented in the figure by the magenta line with diamond marker), and ideally, should be able to reduce MSE values for the particular images as low as possible.

As can be seen from Fig. 9, at high SDI value i.e. high turbidity, all the restoration methods can successfully restore the original underwater image, by giving SDI values lower than that of the original image. However, as SDI is reduced (by reducing turbidity), He *et al.* (2011), Ancuti *et al.* (2012), Codevilla *et al.* (2016) and Galdran *et al.* (2015), fail to effectively restore underwater

Table 4 Average UCIQE and UIQM score on Li *et al.* (2019) dataset

Methods	UCIQE	UIQM
Ancuti <i>et al.</i> (2012)	0.6305	0.6312
Fu <i>et al.</i> (2014)	0.6062	1.4338
Drews <i>et al.</i> (2016)	0.5852	<b>1.6297</b>
Li <i>et al.</i> (2017) (Hybrid)	0.5971	1.2996
Peng <i>et al.</i> (2018)	0.5993	1.4301
Galdran <i>et al.</i> (2015)	0.5421	1.2147
Li <i>et al.</i> (2016)	<b>0.6778</b>	1.5440
Peng and Cosman (2017)	0.6001	1.3757
Proposed Method	0.6414	1.6097

images below certain SDI values; showing an increase, rather than decrease, of MSE value with their restoration methods. He *et al.* (2011) fails to effectively restore underwater images with SDI values of less than 0.07, whilst Ancuti *et al.* (2012) and Codevilla *et al.* (2016) perform better; failing only to restore underwater images with SDI values of less than 0.055. Galdran *et al.* (2015) only fails to reduce MSE of the original image at SDI values of less than 0.012. On the other hand, the proposed restoration method is successful in reducing MSE even at a low value of SDI. In fact, the proposed restoration method is the only restoration method that is capable of reducing MSE over all ranges of SDI and hence, over all turbidity levels. Since Peak Signal to Noise Ratio (PSNR) is inversely proportional to MSE, it can also be derived that the proposed method would also give a good PSNR.

Admittedly, other restoration methods do manage to outperform the proposed restoration method above certain SDI values. At SDI of just above 0.08, both Codevilla *et al.* (2016), and Galdran *et al.* (2015) manage to outperform the proposed method by giving lower MSE values, whilst He *et al.* (2011) and Ancuti *et al.* (2012) outperform the proposed method at SDI value above 0.065. However, the ability of the proposed restoration method to consistently improve the underwater image with different turbidity levels, makes the proposed restoration method an attractive proposal to be adopted for underwater applications, which by its very nature, will temporally and spatially, vary.

In Table 4, two non-reference metrics namely; UCIQE (Yang and Sowmya 2015) and UIQM (Panetta *et al.* 2016), have been used to compare the performance of the proposed restoration method against other restoration methods, based on an image dataset from Li *et al.* (2019). The proposed restoration method performs well, in terms of UCIQE scores, as compared to other restoration methods, except for Li *et al.* (2016). The highest UCIQE score of 0.6778 is obtained by Li *et al.* (2016), followed by the proposed restoration method with UCIQE scores of 0.6414. In terms of UIQM, which is more consistent with human perception, the proposed restoration method supersedes Li *et al.* (2016), with a high UIQM score of 1.6097. This UIQM score is higher as compared to other restoration methods, except for Drews *et al.* (2016), with an UIQM score of 1.6297.

Drews *et al.* (2016) have the highest UIQM score among all the methods considered. But it cannot handle backscattering effects in an underwater image, which reduce contrast, produce a foggy effect in an image, and entirely affecting the object of interest. It also fails to restore images, which are affected by high backscattering effects; with the image selected from Li *et al.* (2019) dataset and given in Fig. 8, being one of the examples. However, the number of such images with backscattering

effects and distortions, are comparatively less in Li *et al.* (2019) dataset, which increases the score of Drews *et al.* (2016). Other restoration methods show results that produce lower performance. This indicates that the proposed method performs well on all kinds of lightings, variations, color dependencies, color tints, and scene configurations, when compared to the other methods.

## 5. Conclusions

In this paper, a novel methodology to restore underwater images taken in challenging underwater environments has been proposed. This is done by estimating the depth map using blurriness estimation, red light intensity and back ground light neutralization process; before using the estimated depth map to estimate transmission map, by accounting for direct and backscattering signals. The estimated transmission map and background light estimation are then used to restore the final scene radiance.

Qualitative and quantitative analysis have been performed on the restored underwater images using the proposed method. The results produced by the proposed method have been compared with many state-of-the-art methods that are available in the literature. It has been shown, qualitatively, that the proposed method can effectively restore underwater images with varying underwater conditions, including open scene underwater images, bluish and greenish images, as well as challenging underwater images affected by backscattering effects. Artificial illumination problem is also handled gracefully due to the background light neutralization method. For quantitative evaluation, four different quality metrics that measure the recovery of edges, restoration quality, amount of error and color quality of a restored image, have been used. In terms of visibility recovery and restoration quality coefficients, the proposed method performs the best among the considered restoration methods. It has been shown that the proposed restoration method is the only restoration methods that can reduce the amount of error from underwater images, and effectively restore underwater images over all range of turbidity; proving the flexibility of the method. The proposed method also performs well on the color quality scores, as compared to other restoration methods.

Although, the underwater images used for testing the proposed method have different color dominances, artificial illumination and various scene configurations, it is agreeable that it is impossible to include images that cover the entire range of underwater conditions that includes different coastal and oceanic water types, sources of errors causing distortions, depth from different viewpoints and other large factors, for testing the proposed restoration method. However, a good number of underwater images with varying conditions had been used to test the proposed restoration method outside the confinement of this paper, with focus given on the most challenging underwater images in this paper, to highlight the effectiveness of the proposed method. These demonstrate that the proposed restoration method is significant, and can be used to provide high quality underwater images for various oceanic activities.

## References

- Akkaynak, D. and Treibitz, T. (2018), "A Revised Underwater Image Formation Model", *Proceedings of the IEEE Conference on Computer Vision and Pattern Recognition*, Salt Lake City, USA, June.
- Ancuti, C., Ancuti, C.O., Haber, T. and Bekaert, P. (2012), "Enhancing underwater images and videos by fusion", *Proceedings of the IEEE Conference on Computer Vision and Pattern Recognition*, Providence,

- USA, June.
- Anwar, S., Li, C. and Porikli, F. (2018), "Deep underwater image enhancement". <https://arxiv.org/abs/1807.03528>.
- Bo, L. (2016), "An adaptive method of multi-scale edge detection for underwater image", *Ocean Syst. Eng.*, **6**(3), 217-231. <http://dx.doi.org/10.12989/ose.2016.6.3.217>.
- Bo, L. and Yan, L. (2012), "A method for underwater image analysis using bi-dimensional empirical mode decomposition technique", *Ocean Syst. Eng.*, **2**(2), 137-145. <http://dx.doi.org/10.12989/ose.2012.2.2.137>.
- Carlevaris, B.N., Mohan, A. and Eustice, R.M. (2010), "Initial results in underwater single image dehazing", *Proceedings of the IEEE OCEANS*, Seattle, USA, September.
- Chang, H., Cheng, C. and Sung, C. (2019), "Single Underwater Image Restoration Based on Depth Estimation and Transmission Compensation", *IEEE J. Oceanic Eng.*, **44**(4), 1130-1149. <https://doi.org/10.1109/JOE.2018.2865045>.
- Chiang, J. Y. and Chen, Y. (2012), "Underwater image enhancement by wavelength compensation and dehazing", *IEEE T. Image Process.*, **21**(4), 1756-1769. <https://doi.org/10.1109/TIP.2011.2179666>.
- Codevilla, F., Gaya, J., Duarte, A. and Botelho, S. (2016), "General Participative Media Single Image Restoration", *Computer Vision and Pattern Recognition*, arXiv:submit/1493653 [cs.CV].
- Drews, Jr., Nascimento, E., Moraes, F., Botelho, S. and Campos, M. (2013). "Transmission estimation in underwater single images", *Proceedings of the IEEE International Conference on Computer Vision Workshops*, Sydney, Australia, December.
- Drews, P.L.J., Nascimento, E.R., Botelho, S.S.C. and Campos, M.F. (2016), "Underwater depth estimation and image restoration based on single images", *IEEE Comput. Graphic. Appl.*, **36**(2), 24-35. <https://doi.org/10.1109/MCG.2016.26>.
- Duarte, A., Codevilla, F., Gaya, J. and Botelho, S. (2016), "A dataset to evaluate underwater image restoration methods", *Proceedings of the IEEE OCEANS*, Shanghai, China, April.
- Fabbri, C., Islam, M.J. and Sattar, J. (2018), "Enhancing underwater imagery using generative adversarial networks", *Proceedings of the IEEE International Conference on Robotics and Automation*, Brisbane, Australia, May.
- Fu, X., Zhuang, P., Huang, Y., Liao, Y., Zhang, X. and Ding, X. (2014), "A Retinex-based enhancing approach for single underwater image", *Proceedings of the IEEE International Conference on Image Processing*, Paris, France, October.
- Galdran, A., Pardo, D., Picon, A. and Alvarez-Gila, A. (2015), "Automatic Red-Channel underwater image restoration", *J. Visual Commun. Image Represent.*, **26**, 132-145. <https://doi.org/10.1016/j.jvcir.2014.11.006>
- Garcia, R. and Gracias, N. (2011), "Detection of interest points in turbid underwater images", *Proceedings of the IEEE oceans*, Santander, Spain, June.
- Gould, R.W., Arnone, R.A. and Martinolich, P.M. (1999), "Spectral dependence of the scattering coefficient in case 1 and case 2 waters", *Appl. Opt.*, **38**(12), 2377-2383. <https://doi.org/10.1364/AO.38.002377>.
- Lu, H., Li, Y., Kim, H. and Serikawa, S. (2017), "Underwater Light Field Depth Map Restoration Using Deep Convolutional Neural Fields", *Proceedings of the International Symposium on Artificial Intelligence and Robotics*, Kitakyushu, Japan, November.
- Hautiere, N., Tarel, J.P., Didier, A. and Dumont, E. (2008), "Blind Contrast Enhancement Assessment by Gradient Rationing at Visible Edges", *Image Anal. Stereology*, **27**, 87-95. <https://doi.org/10.5566/ias.v27>.
- He, K., Sun, J. and Tang, X. (2011), "Single Image Haze Removal Using Dark Channel Prior", *IEEE T. Pattern Anal. Machine Intelligence*, **33**(12), 2341-2353. <https://doi.org/10.1109/TPAMI.2010.168>.
- He, K., Sun, J. and Tang, X. (2013), "Guided Image Filtering", *IEEE Transactions on Pattern Analysis and Machine Intelligence*, **35**(6), 1397-1409. <https://doi.org/10.1109/TPAMI.2012.213>.
- Jarina R.A., Emeroylariffion A. and Silva, L.C.De. (2019), "Review of underwater image restoration algorithms", *IET Image Process.*, **13**(10), 1587-1596. <http://dx.doi.org/10.1049/iet-ipr.2019.0117>.
- Jarina R.A., Emeroylariffion A. and Silva, L.C.De. (2020), "Depth estimation for underwater images from single view image", *IET Image Process.*, **14**(16), 4188-4197. <http://dx.doi.org/10.1049/iet-ipr.2019.1533>.
- Li, C., Guo, J., Chen, S., Tang, Y., Pang, Y. and Wang, J. (2016), "Underwater image restoration based on minimum information loss principle and optical properties of underwater imaging", *Proceedings of the*

- IEEE International Conference on Image Processing*, Arizona, USA, September.
- Li, C., Chunle, G., Ren, W., Cong, R., Hou, J., Kwong, S. and Tao, D. (2019), "An underwater image enhancement benchmark dataset and beyond", *IEEE T. Image Process.*, **29**, 4376-4389. <https://doi.org/10.1109/TIP.2019.2955241>.
- Li, C., Guo, J., Chunle, G., Cong, R. and Gong, J. (2017), "A hybrid method for underwater image correction", *Pattern Recog. Lett.*, **94**, 62-67. <https://doi.org/10.1016/j.patrec.2017.05.023>
- Li, J.A., Skinner, K., Eustice, R. and Johnson-Roberson, M. (2017), "WaterGAN: Unsupervised generative network to enable real-time color correction of monocular underwater images", *IEEE Robot. Autom. Lett.*, 1-8. <https://doi.org/10.1109/LRA.2017.2730363>.
- Liu, C. and Meng, W. (2010), "Removal of water scattering", *Proceedings of the International Conference on Computer Engineering and Technology*, Chengdu, China, April.
- Narasimhan, S.G. and Nayar, S.K. (2002), "Vision and the Atmosphere", *Int. J. Comput. Vision*, **48**(3), 233-254. <https://doi.org/10.1023/A:1016328200723>.
- Panetta, K., Gao, C. and Agaian, S. (2016), "Human-Visual-System-Inspired Underwater Image Quality Measures", *IEEE J. Oceanic Eng.*, **41**(3), 541-551. <https://doi.org/10.1109/JOE.2015.2469915>.
- Peng, Y. and Cosman, P.C. (2017), "Underwater Image Restoration Based on Image Blurriness and Light Absorption", *IEEE T. Image Process.*, **26**(4), 1579-1594. <https://doi.org/10.1109/TIP.2017.2663846>.
- Peng, Y., Zhao, X. and Cosman, P.C. (2015), "Single underwater image enhancement using depth estimation based on blurriness", *Proceedings of the IEEE International Conference on Image Processing*, Quebec City, Canada, September.
- Peng, Y.T., Cao, K. and Cosman, P. (2018), "Generalization of the dark channel prior for single image restoration", *IEEE T. Image*, **27**(6), <https://doi.org/10.1109/TIP.2018.2813092>.
- Roser, M., Dunbabin, M. and Geiger, A. (2014), "Simultaneous underwater visibility assessment, enhancement and improved stereo", *Proceedings of the IEEE International Conference on Robotics and Automation*, Hong Kong, China, May.
- Schechner, Y. Y. and Karpel, N. (2005), "Recovery of underwater visibility and structure by polarization analysis", *IEEE J. Oceanic Eng.*, **30**(3), 570-587. <https://doi.org/10.1109/JOE.2005.850871>.
- Serikawa, S. and Lu, H. (2013), "Underwater image dehazing using joint trilateral filter", *Comput. Elec. Eng.*, **40**. <https://doi.org/10.1016/j.compeleceng.2013.10.016>.
- Shanmugam, P., Sundarabalan, B., Ahn, Y. and Ryu, J. (2011), "A New inversion model to retrieve the particulate backscattering in coastal/ocean waters", *IEEE T. Geosci. Remote Sens.*, **49**(6), 2463-2475. <https://doi.org/10.1109/TGRS.2010.2103947>.
- Shin, Y., Cho, Y., Pandey, G. and Kim, A. (2016), "Estimation of ambient light and transmission map with common convolutional architecture", *Proceedings of the IEEE OCEANS Monterey*, USA, September.
- Simon E., Lars C. and Andrea C. (2015), "Hierarchical rank-based veiling light estimation for underwater dehazing", *Proceedings of the British Machine Vision Conference*, Swansea, UK, January.
- Smith, R. and Baker, K. (1981), "Optical properties of the clearest natural waters (200–800 nm)", *Appl. Opt.*, **20**, 177-184. <https://doi.org/10.1364/AO.20.000177>.
- Solonenko, M.G. and Mobley, C.D. (2015), "Inherent optical properties of Jerlov water types", *Appl. Opt.*, **54**(17), 5392-5401. <https://doi.org/10.1364/AO.54.005392>.
- Tan, C.S., Sluzek, A., Seet, G.L., G. and Jiang, T.Y. (2006), "Range gated imaging system for underwater robotic vehicle", *Proceedings of the IEEE Oceans*, Singapore, May.
- Wang, K., Hu, Y., Chen, J., Wu, X., Zhao, X. and Li, Y. (2019), "Underwater Image Restoration Based on a Parallel Convolutional Neural Network", *Remote Sens.*, **11**, 1591-1611. <http://dx.doi.org/10.3390/rs11131591>.
- Wen, H., Tian, Y., Huang, T. and Gao, W. (2013), "Single underwater image enhancement with a new optical model", *Proceedings of the IEEE International Symposium on Circuits and Systems*, Beijing, China, May.
- Whitmire, A., Boss, E., Cowles, T. and Pegau, W. (2007), "Spectral variability of the particulate backscattering ratio", *Optics Express*, **15**, 7019-7031. <https://doi.org/10.1364/OE.15.007019>.
- Yang, H., Chen, P., Huang, C., Zhuang, Y. and Shiau, Y. (2011), "Low complexity underwater image enhancement based on dark channel prior", *Proceedings of the International Conference on Innovations in*

- Bio-inspired Computing and Applications*, Shenzhen, China, December.
- Yang, M. and Sowmya, A. (2015), "An underwater color image quality evaluation metric", *IEEE T. Image Process.*, **24**(12), 6062-6071. <https://doi.org/10.1109/TIP.2015.2491020>.
- Zhang, M. and Peng, J. (2018), "Underwater image restoration based on a new underwater image formation model", *IEEE Access*, **6**, 58634-58644. <https://doi.org/10.1109/ACCESS.2018.2875344>.
- Zhao, X., Jin, T. and Qu, S. (2015), "Deriving inherent optical properties from background color and underwater image enhancement", *Ocean Eng.*, **94**, 163-172. <https://doi.org/10.1016/j.oceaneng.2014.11.036>.
- Zhishen, L., Tianfu, D. and Gang, W. (2003), "ROV based underwater blurred image restoration", *J. Ocean Univ. Qingdao*, **2**, 85-88.
- Zhou, W., Bovik, A.C., Sheikh, H.R. and Simoncelli, E.P. (2004), "Image quality assessment: from error visibility to structural similarity", *IEEE T. Image Process.*, **13**(4), 600-612. <https://doi.org/10.1109/TIP.2003.819861>.

AK